

Application of different molecular sieves in photothermal catalysis of *Jatropha* oil

Yijie Yang¹, Longlong Ma^{1,2}, Lumin Sun³, Xinghua Zhang², Chao Gui¹, Yubao Chen^{1*}

(1. School of Energy and Environmental Science, Yunnan Normal University, Kunming 6500500, China;

2. School of Energy and Environment, Southeast University, Nanjing 210096, China;

3. School of Environmental Science and Engineering, Tan Kah Kee College, Xiamen University, Zhangzhou 363105, Fujian, China)

Abstract: The preparation of green and economical bio-aviation fuel is a priority for the sustainable development industry. In this study, *Jatropha* oil was used as a raw material to catalyze the conversion of raw material to aviation kerosene fraction by photothermal coupling under the conditions of light and low temperature. The correlations among conversion rate, target alkane selectivity, composition distribution, and catalyst microstructure were investigated by X-ray diffraction (XRD), high-resolution transmission electron microscopy (HRTEM), nitrogen (N₂) adsorption and desorption, X-ray fluorescence (XRF), ammonia-temperature programmed desorption (NH₃-TPD), ultraviolet-visible spectrophotometry (UV-Vis), and other characterization. The correlation between conversion and target alkane selectivity and composition distribution and catalyst microstructure was investigated, and different modification methods and different molecular sieve materials were selected. The results showed that the molecular sieves modified with the solid dispersion method could retain the structural stability of titanium dioxide (TiO₂) and molecular sieves to a great extent while slightly enhancing the pore capacity and pore size of the catalyst to make it easier to adsorb reactants; the introduction of active metal platinum (Pt) could reduce the forbidden bandwidth of the catalyst, increase the weak acid amount of the catalyst, improve the adsorption capacity of hydrogen (H₂), and thus improve the catalytic ability, resulting in a suitable catalyst for this study: P-21. The photothermal catalytic reaction of *Jatropha* oil using P-21 catalyst obtained 97.21% conversion and 74.99% selectivity of the target alkanes under the optimal process parameters. The results of this study provide effective catalyst parameters for research in the field of clean energy

Keywords: *Jatropha* oil, applications of molecular sievers, photothermal catalysis, biofuel

DOI: [10.25165/ijabe.20231606.7635](https://doi.org/10.25165/ijabe.20231606.7635)

Citation: Yang Y J, Ma L L, Sun L M, Zhang X H, Gui C, Chen Y B. Application of different molecular sieves in photothermal catalysis of *Jatropha* oil. *Int J Agric & Biol Eng*, 2023; 16(5): 204–212.

1 Introduction

The world's energy demands depend primarily on fossil resources. China's fossil fuel energy relies on coal, oil, and gas. Coal is the main energy source in China. Limited resources, decreasing crude oil resources, and increasing oil demand are further exacerbating environmental problems, such as the greenhouse effect brought about by the use of fossil fuels. Therefore, developing and exploring renewable energy has become imperative^[1-3]. Additionally, the 14th Five-Year Plan has noted that in future development, energy, as a guarantee of infrastructure and economic development, faces the constraint of "carbon peaking and carbon neutrality." According to the International Energy Agency, transportation is the second largest carbon-emitting sector in the world, accounting for 25% of carbon emissions, with global aviation emissions accounting for 2.6% of all human-made carbon

dioxide (CO₂) emissions^[4,5]. Hence methods need to be developed to decrease the total carbon emissions, which has led to an increasing interest in the use of biofuels^[6]. Biomass is an important source for producing biofuels, which have the advantage of being a sustainable energy source compared with petroleum-based fuels and can reduce the greenhouse effect, improve air quality, and reduce dependence on petroleum^[7,8]. Renewable aviation fuels derived from biomass have provided a sustainable aviation energy option with promising applications^[9].

The main constituents of aviation kerosene are C₈-C₁₆ straight-chain alkanes, branched-chain alkanes, and aromatic hydrocarbons. Fatty acid triglycerides are the major component in most vegetable oils and their carbon chain number varies from 10 to 20. Fatty acid triglycerides can be converted into C₈-C₁₆ alkanes by hydrogenation, deoxidation, and isomerization^[10-12]. Thus, nonedible vegetable oils and fats are ideal materials for the preparation of aviation kerosene. Common raw materials include vegetable oils extracted from oilseed crops, such as soybean, rapeseed, castor, *Jatropha*, or plants with high oil content^[13-16]. The preparation methods of aviation kerosene include Fischer-Tropsch synthesis^[4,9], fatty acid esterification technology, catalytic hydrogenation technology, alkane cracking and isomerization technology, and photothermal catalysis^[17-19]. Hydrocatalysis holds significant interest because of its fast reaction and high yield^[20]. The reaction conditions of hydrocatalysis are harsh, however, in order to ensure the yield, the reaction must be carried out under high temperature and high hydrogen pressure. As a result, the production process consumes a lot of hydrogen and electricity, and this process also has a negative

Received date: 2022-04-25 **Accepted date:** 2023-02-28

Biographies: Yijie Yang, MS candidate, research interest: photocatalysis of biomass, Email: yy1045858516@163.com; Longlong Ma, PhD, Professor, research interest: renewable energy, mall@seu.edu.cn; Lumin Sun, PhD, Professor, research interest: pollutant transport analysis, sunlumin@xmu.edu.cn; Xinghua Zhang, PhD, Professor, research interest: biobased-fuel preparation, Email: zhangxh@seu.edu.cn; Chao Gui, MS candidate, research interest: biomass pyrolysis analysis, Email: 2551007805@qq.com.

***Corresponding author:** Yubao Chen, PhD, Professor, research interest: cleaner production, photocatalysis of biomass, biobased jet-fuel preparation. School of Energy and Environmental Science, Yunnan Normal University, Kunming 6500500, China. Tel: +86-13888821945, Email: chenyubao@ynnu.edu.cn.

impact on the environment. Therefore, the development of a method to prepare aviation kerosene under mild conditions has become a popular research topic in recent years.

Catalysis is a central element in the production of fuels from non-food biomass. At present, photocatalysis has been used widely in the fields of hydrogen production, CO₂ reduction, and removal of volatile organic compounds. Anatase titanium dioxide (TiO₂) has become the most employed photocatalyst because of its inherent superior photocatalytic properties. Under UV irradiation, TiO₂ can decarboxylate short-chain fatty acids. Although the study of decarboxylation of triglycerides of long-chain fatty acids has not yet been carried out in-depth, theoretically, it is completely feasible. Studies on the improvement of light absorption and photocatalytic performance of anatase TiO₂ have focused mainly on the enhancement of photoactivity by doping modification with cations or anions, usually by adding noble metals, such as Pt, Pd, Ir, and Ag, which act as electron capture centers, to the semiconductor surface^[21].

To investigate the effect of molecular sieves on photothermal catalysis in composite catalytic materials, in this study, a novel method for the preparation of aviation kerosene by photothermal coupling catalysis of Jatropha oil was proposed, using commercial P25 TiO₂ and commercial molecular sieve as raw materials and Jatropha oil as the research object. The preparation experiments of aviation kerosene were completed under the conditions of low temperature and low hydrogen pressure. The optimum catalyst and reaction conditions for the photothermal coupling catalytic experiments were derived and reasonably deduced the reaction paths, which provided some ideas for the preparation of aviation kerosene under mild conditions.

2 Materials and methods

2.1 Materials

Jatropha oil was purchased from Huakun Co., Ltd., Xishuangbanna, Yunnan Province, China. The gas chromatography-mass spectrometry (GC-MS) analysis of Jatropha oil is listed in Table 1. The main fatty acids in Jatropha oil are oleic acid, linoleic acid, and palmitic acid.

Table 1 Main components of Jatropha oil

Composition	Chemical equation	Relative content/%
Oleic acid/linoleic acid	C ₁₈ H ₃₄ O ₂ /C ₁₈ H ₃₂ O ₂	86.720
Palmitic acid	C ₁₆ H ₃₂ O ₂	8.390
Others	-	4.890

The gas was purchased for the experiment from Kunming Canghui Trade Gas Co., Ltd., Yunnan Province, China. The usage is listed in Table 2.

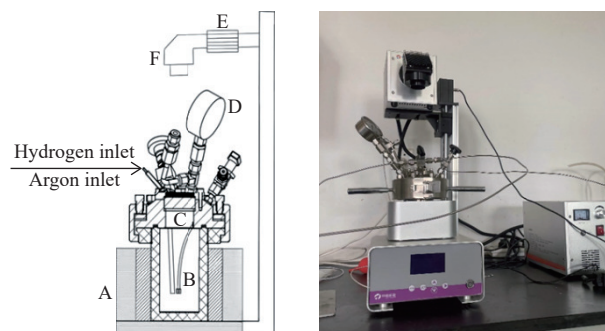
Table 2 Usage of the gas in this study

Gas	Specification	usage
Hydrogen (H ₂)	≥99.999%	Source of hydrogen
Argon (Ar)	≥99.999%	Remove air from the reactor
Helium (He)	≥99.999%	carrier gas

2.2 Main instruments

A photothermal catalytic reactor equipped with scratch-resistant sapphire that allows 99% of the incident light to pass through guaranteed that the catalyst could be fully illuminated (as shown in Figure 1). The reactor was designed and manufactured by CEALIGHT Mechanical Equipment Co. Ltd., Beijing, China. The

manufacturer's details of the remaining equipment are as follows: CEL-HXF300-T3 xenon lamp system was employed to simulate solar light (radiant output: 50 W, UV output: 2.6 W, IR output: 28.8 W, visible output: 5000 lm, spectral output: 320-2500 nm);



Note: A. Control panel and heating element; B. Reaction tank; C. Scratch-resistant sapphire window; D. Pressure meter; E. Xenon lamp system; F. Retroreflector

Figure 1 Structure and photo of the photothermal catalytic reactor

2.3 Methods

2.3.1 Preparation of Pt/TiO₂ catalysts

The preparation of Pt/TiO₂ catalysts used K₂PtCl₄ aqueous solution as the metal precursor by impregnating the load with 1 wt.% Pt. Dispersed by ultrasound was slowly added into TiO₂ and left to dry for 12 h at 85°C. The dried powder was heated to 400°C in a muffle furnace at a rate of 10°C/min. The catalyst was kept at this temperature for 4 h and then ground to 60 mesh. Finally, the Pt/TiO₂ catalyst was obtained^[7].

2.3.2 Preparation of Pt/TiO₂-S

The solid dispersion method was used to prepare the TiO₂-molecular sieve composites. To prepare the TiO₂-HZSM-5 materials, HZSM-5 was dispersed in 20 mL isopropyl alcohol and stirred at room temperature for 1 h. Next, the same weight of P25 TiO₂ was added to the slurry and then stirred at room temperature for 12 h. Then the slurry was put in an oven, and the samples were calcined in a muffle furnace at 400°C for 4 h at a rate of 10°C/min and then ground to 60-mesh. Finally, TiO₂-HZSM-5 materials were obtained. The active metal (Pt) on top of TiO₂-HZSM-5 was loaded by impregnation and was labeled as Pt/TiO₂-HZSM-5 (P-21), Pt/TiO₂-HZSM-5 (P-60), Pt/TiO₂-HZSM-5 (P-130), and Pt/TiO₂-SAPO-11 (P-11), Pt/TiO₂-Al-MCM-41 (P-41) with different Si/Al ratio were prepared in the same way as P-21.

2.3.3 Preparation of solvent-gel catalysts

The solvent-gel catalyst was prepared as follows: 3.0 g of HZSM-5 molecular sieve was submerged in 45 mL of isopropanol and mixed for 1.0 h. The molecular sieve slurry was dispersed by ultrasound for 0.5 h to form a uniformly dispersed molecular sieve slurry. Tetrabutyl titanate with 50% molecular sieve mass fraction (in terms of TiO₂) was added dropwise to the molecular sieve slurry. After the titanium precursors were completely dissolved, 1 mL of glacial acetic acid was added to adjust the solution pH of the mixed system, and the mixing was continued for 1 h. Finally, a certain amount of deionized water (molar ratio of TBOT: H₂O is 1:15) was slowly added drop by drop and hydrolyzed for 2 h. After the completion of hydrolysis, the products were centrifuged, washed with anhydrous ethanol, and dried, which was followed by calcination at 400°C to remove the organic matter to obtain TiO₂-modified HZSM-5 molecular sieves. The solvent-gel type Pt/TiO₂-HZSM-5 (PG) was obtained by loading the material with active metals by impregnation.

2.3.4 Catalyst characterization

An XRD was equipped with Cu-K α radiation ($\lambda=0.154$ nm), operating at 36 kV and 30 mA. The samples were scanned in the range of 5° to 90° at a rate of 10°/min. XRF was operated at 60 kV and 40 MA using Rh radiation.

The sample was dispersed in ethanol solution, sonicated for 3 min, and then added drop by drop onto an ultrathin carbon film for HRTEM observation.

For CO pulse chemisorption, 50 mg of the catalyst was ground to 40-60 mesh in a U-shaped quartz tube and cooled down to 350°C for 2.0 h under 10% H₂/Ar atmosphere. Then, Helium (He) was continuously injected for 0.5 h to lower the temperature to 50°C. Finally, 10% CO/He was introduced for pulse adsorption until the pulse signal was stable.

To prepare the samples for NH₃-TPD, the samples were first placed at 350°C under 10% H₂/Ar atmosphere for 2 h. When the temperature dropped to 100°C, 10% NH₃/He was added at a flow rate of 20 mL/min for 1 h. He was used to remove the physically adsorbed NH₃, and the temperature increased from 100°C to 800°C at a rate of 10°C/min.

For N₂ desorption-adsorption, a certain number of samples for 180 min under vacuum at 300°C. The data were collected in a sample tube in a liquid nitrogen atmosphere.

The composition of liquid products was detected by GC-MS. A CETM-5 column (30.00 m \times 0.25 mm \times 0.25 μ m) was used, and the injection temperature was 250°C. The temperature program was as follows: the initial temperature was 80°C and held for 2 min; heated to 130°C at 5°C/min and held for 5 min; heated to 180°C at 5°C/min and held for 5 min; and heated to 230°C at 5°C/min and held for 5 min. The carrier gas (He) flow rate was 1.0 mL/min. The MS conditions were as follows: electron bombardment (EI) ion source with an electron energy of 70 eV, a temperature of 250°C, a transmission line temperature of 270°C, a detection voltage of 0.9 kV, a mass scan range of 60-500 m/z, and a data acquisition time of 4.20-47.00 min.

2.4 Calculation methods

The liquid products are mainly composed of saturated alkanes. The results of the GC-MS analysis were compared with the NIST (National Institute of Standards and Technology) standard spectral library. The qualitative analysis was the relative retention, and the quantitative analysis was the corrected area normalization. In the data processing system, the area normalization method was used for quantitative analysis, and the relative percentage of each alkane component was obtained. The C₈-C₁₇ alkane was the main product of the reaction.

The selectivity of C₈-C₁₇ alkanes is calculated as Equation (1).

$$X = \sum M_{(x)} / [M_{(T0)} - M_{(TG)}] \times 100\% \quad (1)$$

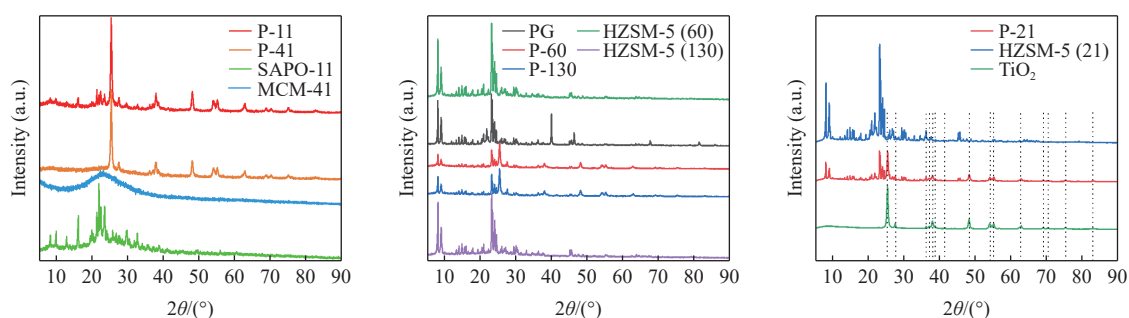


Figure 2 XRD characterization of catalytic materials

where, X is the selectivity of C₈-C₁₇ alkanes, %; $M_{(x)}$ is the total mass percentage of C₈-C₁₇ alkanes in the liquid products, %; $M_{(T0)}$ is the mass percentage of Jatropa oil before the reaction; $M_{(TG)}$ is the mass percentage of Jatropa oil after the reaction.

The feedstock conversion rate is calculated as Equation (2).

$$Y = [M_{(T0)} - M_{(TG)}] / M_{(T0)} \times 100\% \quad (2)$$

where, Y is the feedstock conversion rate, %. The contents of different alkanes in total alkanes are calculated as Equation (3).

$$Z = \sum M_{(y0)} / M_{(y)} \times 100\% \quad (3)$$

where, Z is the contents of different alkanes in total alkanes, %; $M_{(y0)}$ is the mass percentage of one alkane after the reaction; $M_{(y)}$ is the total alkane content after the reaction.

3 Results and discussion

3.1 Textural and morphological properties of catalysts

The XRD spectra of P-21, P-60, P-130, P-11, P-41, PG catalysts, and premodified materials are shown in Figure 2. The characteristic diffraction peaks of TiO₂ were observed at $2\theta=25.281^\circ$, 37.8° , 38.575° , 48.049° , 53.89° , 55.06° and 62.74° , corresponding to anatase phase TiO₂ (JCPDS card number: 21-1272); and at $2\theta=27.446^\circ$, 36.085° , 36.946° and 41.225° , corresponding to a small amount of rutile-phase TiO₂ (JCPDS card No. 21-1276)^[22]. In addition, the introduction of Pt showed no obvious characteristic diffraction peaks, probably because of the small particle size of the active metal or the high dispersion of the metal. The total doping of the active metal was only 1%, which also may explain why the XRD characterization analysis could not be further observed. The characteristic diffraction peaks of P-21, P-60, P-130, P-11, and P-41 catalysts corresponded to those of their molecular sieves HZSM-5 (21), HZSM-5 (60), HZSM-5 (130), SAPO-11, and MCM-41^[23]. The intensity of diffraction peaks decreased compared with the original molecular sieve, but the characteristic peaks remained unchanged. This result indicated that the P25 TiO₂ modification and Pt loading did not destroy the crystal structure of the molecular sieve, and the molecular sieve maintained the intact MFI topology. Compared with the solid dispersion method, the intensity of the diffraction peak of the PG catalyst made by the solvent gel method was significantly reduced. After comparing by standard PDF cards, an obvious diffraction peak appeared on the PG at $2\theta=39.763^\circ$, which probably was bonded between the Ti and Al atoms. According to the previous study, the PG catalytic performance was not good. Therefore, the use of the solid dispersion method to prepare the catalyst was more suitable for this experiment.

The HRTEM images of the catalysts (Figure 3) showed that for the catalysts except PG, TiO₂ was in close contact with the

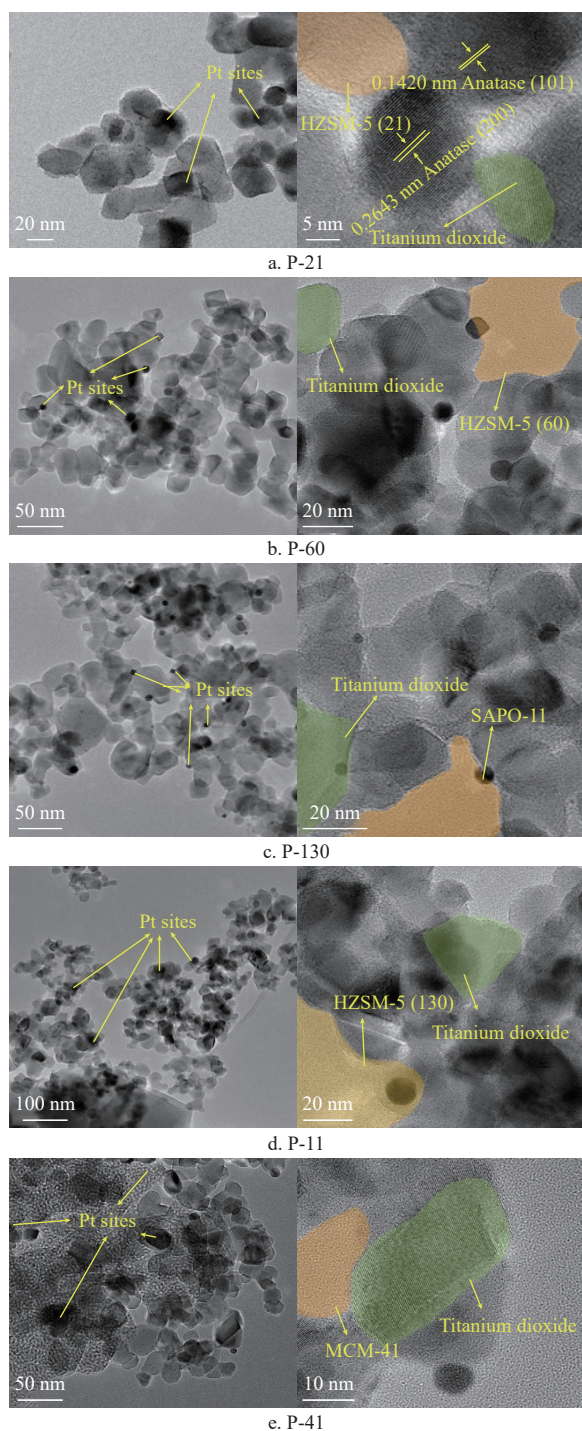
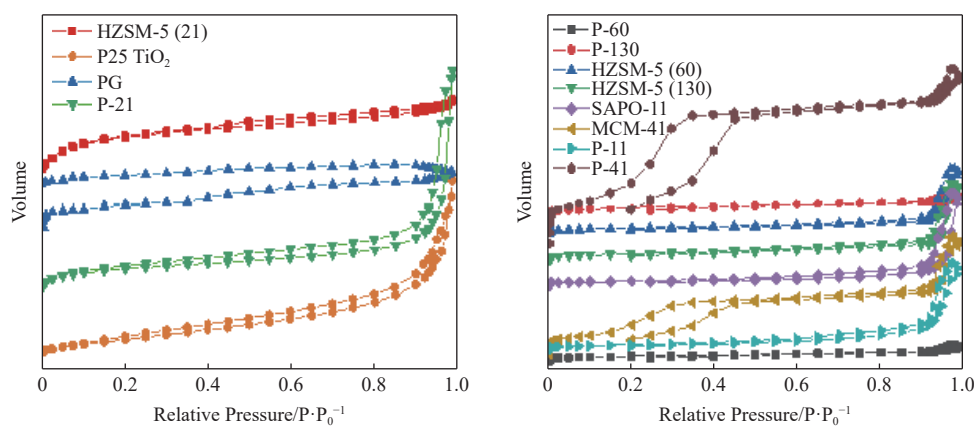


Figure 3 Catalytic material HRTEM picture

Figure 4 N_2 adsorption-desorption isotherms for catalytic materials

molecular sieve. TiO_2 lattice also contains anatase and rutile phases. Pt metal particles were highly dispersed on the surface of the molecular sieve without obvious agglomeration. HRTEM images of the PG catalysts showed faintly visible active metal sites, but some of the sites were blurred, probably because of nanoscale TiO_2 wrapping. The molecular sieve pore channels were not uniformly distributed, presumably because the pore channels were blocked by some substance, which resulted in the Pt precursor solution not being able to diffuse well on TiO_2 -HZSM-5. According to previous studies, for photothermal catalysts, the dispersion and particle size of the active metal affect the mass transfer of the intermediates, and the highly dispersed active metal with smaller particle size exhibits higher catalytic activity^[24]. The grain size of the metal-doped on conventional molecular sieves was generally distributed between 8-30 nm with a dispersion of about 25%, whereas the average particle size of the active metals of P-21 was 1.79 nm, with a dispersion more than 45%. This result indicated that the loaded TiO_2 facilitated the metal molecular sieve surface dispersion^[25,26].

The specific surface area and pore structure of the carriers are closely related to the catalytic reaction. The size of the surface area plays an important role in the dispersion of the active metal, and the pore structure affects the selectivity of the directed products of the catalyst^[27]. The specific surface area and pore structure distribution of the catalysts were analyzed by N_2 adsorption and desorption characterization (Figure 4). The surface area was obtained by the Brunauer-Emmett-Teller (BET) method, the pore volume was obtained by the t-plot method, and the average pore size was obtained by density functional theory (DFT) calculation^[28]. According to the classification of the International Union of Pure and Applied Chemistry (IUPAC), HZSM-5 (21) exhibited a type I adsorption isotherm curve; SAPO-11 and MCM-41 exhibited a type IV adsorption isotherm curve, and pure P25 TiO_2 exhibited a type II isothermal curve. After being modified by the solid dispersion method, the total specific surface area of the molecular sieve and TiO_2 . The XRD characterization results showed that the catalyst still had the properties of the corresponding molecular sieve. Conversely, the specific surface area, pore capacity, and pore size of the PG catalyst prepared by the solvent gel method decreased because the tetrabutyl titanate solution first infiltrated the surface of the molecular sieve during the preparation process by the SGL method. Then part of the solution entered the interior of the molecular sieve to generate TiO_2 and block the pore channels of the HZSM-5 molecular sieve^[23,27,29]. Therefore, the solid dispersion method was more suitable for this experiment.

3.2 Compositional analysis

XRF was used to determine the catalyst compositions before and after modification, and the results are listed in Table 3. The chemical components of the modified catalysts changed significantly, but the Si/Al ratio did not change significantly, indicating that the structure and components of the catalysts did not change after the modification. In addition, the TiO₂ content of all catalysts except the PG catalyst was about 55%, which was close to the theoretical loading of 50%. In contrast, the TiO₂ content of the PG catalyst was 21.36%, which was significantly different from the theoretical loading. The large loss of TiO₂ precursors during the preparation of the solvent gel method probably led to the deviation of the loading. The active metal content in the modified catalysts was different from the theoretical design value by about 0.3%, which was within the normal range.

Table 3 Distribution of components before and after modification of catalytic materials

Sample	Al ₂ O ₃ / (wt.%)	SiO ₂ / (wt.%)	TiO ₂ / (wt.%)	Load metal/ (wt.%)	Al ₂ O ₃ / SiO ₂
PG	2.45	69.72	21.36	0.71	32.54
P-21	1.73	40.45	54.03	0.77	23.43
P-60	1.16	42.79	54.32	0.74	36.88
P-130	0.40	44.00	54.13	0.67	110.28
P-11	15.07	8.62	57.46	0.69	1.74
P-41	2.14	37.13	58.64	0.73	17.35
HZSM-5 (21)	3.82	95.73	-	-	25.06
HZSM-5 (60)	2.35	97.32	-	-	41.33
HZSM-5 (130)	0.91	98.73	-	-	109.09
SAPO-11	34.82	20.92	-	-	1.66
MCM-41	5.33	93.08	-	-	17.46

The amount of acid is an important factor affecting the cracking of long-chain alkanes. The content of reaction products is affected by variations in the amount of acid. NH₃-TPD was used to investigate the effect of different metal loadings and TiO₂ modifications on the acid type distribution by analyzing the weak (120°C-300°C), medium to strong (300°C-500°C), and strong (500°C-800°C) acid sites on the catalyst, as shown in Figure 5^[30,31].

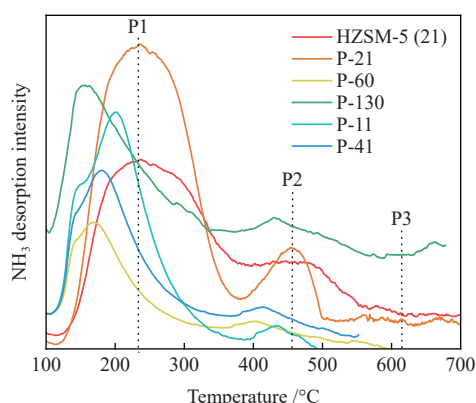


Figure 5 Characterization of catalytic materials NH₃-TPD

The HZSM-5 molecular sieve is widely used in oil and grease hydrogenation, in which the HZSM-5 molecular sieve with low Si/Al ratio exhibits more considerable carboxylic acid and C-C bond-breaking ability^[32]. In this study, an HZSM-5 molecular sieve with a Si/Al ratio of 21 was used, and the NH₃-TPD characterization results indicate that it contains a certain number of acid sites, which would be beneficial for the cracking of long-chain

alkanes.

For P-21 catalysts, three desorption peaks appeared at 240°C (P1), 460°C (P2), and 570°C (P3), which were weak acidic, moderate acidic, and strong acidic sites, respectively. These peaks corresponded to those of the raw material molecular sieve HZSM-5 (21), indicating that the metal loading and P25 TiO₂ modification did not affect the acid distribution of the catalyst. The desorption peak of P-21 was significantly enhanced at 240°C, presumably because of the additional weak acid sites provided by TiO₂, which increased the content of weak acid sites on the catalysts. In addition, the increased peak area enhanced the acidity and catalytic cracking performance of the catalyst. Considering that the test temperature in this study generally was lower than 200°C, this result indicated that the weak acid played a dominant role in the catalytic process. A comparison of the P1 peak areas showed that the P-21 catalyst was larger than the other catalysts. Thus, the P-21 catalyst had the best catalytic effect.

The absorbance values of the modified catalysts and their molecular sieves were using UV-visible spectroscopy in the wavelength range of 200-800 nm. As shown in Figure 6, the P25 TiO₂ material absorbed hardly any visible light, and the TiO₂-HZSM-5(21) material absorbed visible light only in trace amounts. The introduction of the active metal changed the symmetry of the Ti-O-Ti bond, which resulted in more surface lattice defects. The enhancement of the absorbance of P-21 was the most obvious. Although the absorbance of the PG catalyst for visible light was enhanced, the absorbance in the UV band from 200 to 280 nm and the near UV band from 290 to 400 nm was poor. Combined with the XRD analysis, it was found that the photocatalytic performance of the catalysts prepared by the solvent gel method was low.

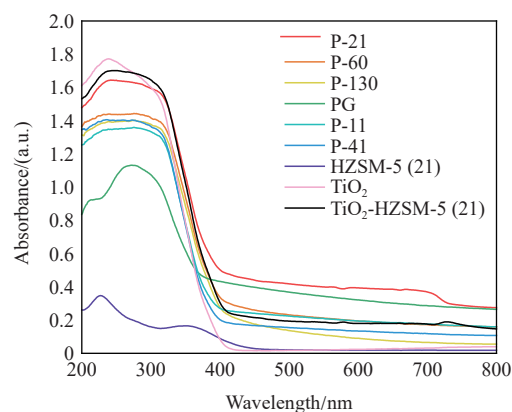


Figure 6 UV-Vis profiles of the samples

3.3 Exploration of the modified catalyst performance

The optimal reaction conditions of this experiment were obtained from a previous research group. The reaction temperature was 100°C, the reaction hydrogen pressure was 0.4 MPa, the rotation speed was 1000 r/min, and the reaction time was 6 h.

3.3.1 Effect of different modification methods on catalyst performance

In this study, HZSM-5 (21) molecular sieve was used as the blank group. The TiO₂-HZSM-5 (21) material was prepared according to the solid dispersion method and solvent gel method. P-21 and PG catalysts were obtained by loading active metal Pt. 0.8 g Jatropa oil and 0.4 g catalyst were mixed with 50 mL n-hexane and then the catalyst was to the reactor. The reaction was performed at 120°C and 0.4 MPa hydrogen pressure for 12 h. The experimental results are shown in Figure 7. It can be observed that the conversion

rate of C_8 - C_{17} alkanes was low with a selectivity of 0% when the reaction was carried out without the catalyst and with heating only. The result indicated that no photothermal catalysis or decarboxylation reaction had taken place. The TiO_2 -HZSM-5 prepared by the solid dispersion method had a catalytic activity of 9.41%, which may be caused by the cracking of long-chain alkanes at the weak acidic site of HZSM-5. Under the same conditions, the alkane conversion and selectivity of PG catalyst were 53.38% and 6.58%, respectively, and were 93.20% and 51.18%, respectively, after P-21 was involved in the reaction. In addition, the molecular sieve prepared by the solvent gel method produced more ester compounds, such as isopropyl linoleate and isopropyl palmitic acid, in the catalytic reaction. Because of the decarboxylation of fatty acids, a large amount of heptadecane and pentadecane was produced in the molecular sieve prepared by the solid dispersion method. This result indicated that the catalytic effect of the modified catalyst prepared by the solid dispersion method was better than that prepared by the solvent gel method.

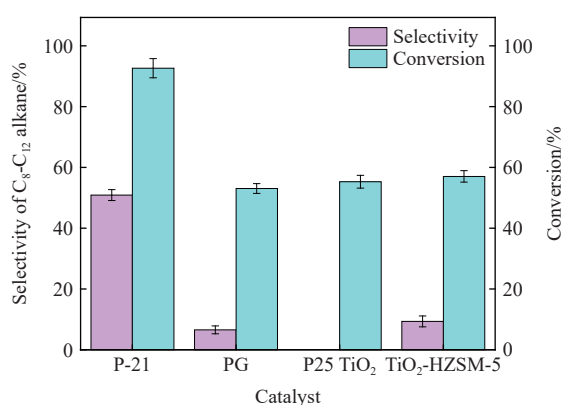


Figure 7 Effect of different compounding methods on the photothermal catalysis of Jatropha oil

3.3.2 Effect of different molecular sieve materials on catalyst performance

The catalytic system used in this study was composed of molecular sieve materials, active metal Pt, and a TiO_2 semiconductor. The molecular sieve had a large number of adjustable acidic sites, a large specific surface area, and good adsorption performance for reactants, which has been widely used in the study of one-step hydrogenation to prepare biofuels. Different physical and chemical properties of molecular sieves have obvious differences, including concrete embodiment in composition, specific surface area, morphology, hole size, hole entrance, and Si/Al ratio. The specific surface area will affect the molecular sieve adsorption of raw materials, the channel will affect the product distribution, and the molecular sieve and Si/Al ratio will affect the amount of acid and acid type. Furthermore, the ratio also will affect the alkane cracking and isomerization process. In this study, HZSM-5, SAPO-11, and MCM-41 molecular sieves were used, and HZSM-5 molecular sieves with Si/Al ratios of 21, 60, and 130 were used to set the Si/Al ratios. The experimental results are shown in Figure 8. According to the catalytic test results of P-21, P-11, and P-41, we concluded that P-21 prepared by HZSM-5 (21) molecular sieve had the best catalytic effect, with >90% conversion rate and >50% alkane selectivity. P-11 and P-41 had high alkane selectivity but a low conversion rate. From the catalytic test results of P-21, P-60, and P-130, the catalytic effect of PTH-21 with a Si/AL ratio of 21 was the best. Therefore, the HZSM-5 molecular sieve with a Si/Al ratio of 21 was the most suitable for this study.

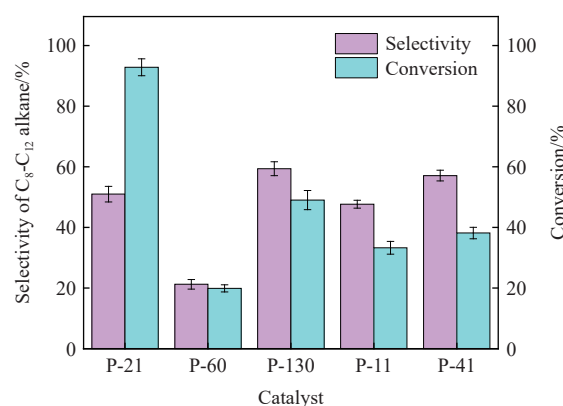


Figure 8 Effect of different molecular sieves on the photothermal catalysis of Jatropha oil

3.3.3 Performance test and analysis of PTH-21 catalyst

To verify the best performance of the catalyst and ensure the accuracy of experimental results, we set up six groups of comparative experiments in this study. The verification experiments included a blank group without a catalyst, the lighting contrast group, the heating contrast group, the P25 TiO_2 contrast group, the TiO_2 -HZSM-5 (21) contrast group, and the PTH-21 catalyst. The results of these experiments are shown in Figure 9.

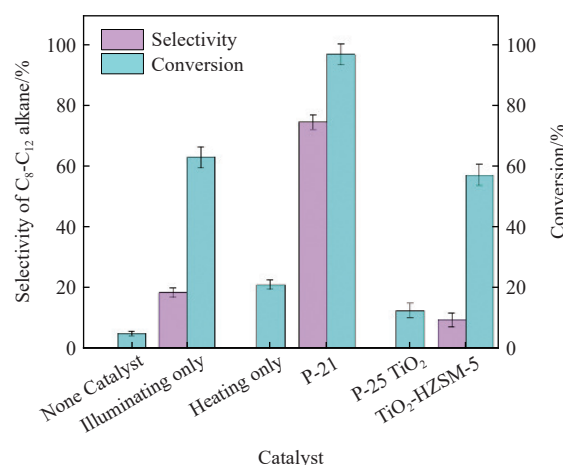


Figure 9 Product distribution of aviation kerosene from Jatropha oil under different conditions

The conversion rate of C_8 - C_{17} alkanes was low in the catalyst-free group, the heated-only group, and the P25 TiO_2 contrast groups, with a selectivity of 0%, indicating that no photothermal catalysis or decarboxylation occurred. After light was added, even at room temperature, the conversion rate of C_8 - C_{17} alkane reached 63.21%, and the selectivity was 18.14%, which indicated that the photocatalytic reaction had occurred. The light condition was the key factor in the reaction, and the reaction was dominated by photocatalytic decarboxylation at a low temperature. In addition, the comparison group of TiO_2 -HZSM-5 (21) obtained a small amount of dodecane, which may have been caused by the cracking of long-chain alkanes at the weak acidic site of HZSM-5. TiO_2 -HZSM-5 (21) catalyst was not doped with an active metal. Thus, the overall conversion rate and selectivity of target alkanes were not high. The conversion rate and selectivity of P-21 catalyst reached 97.21% and 74.99%, and the products were mainly n-dodecane, n-pentadecane, and n-heptane.

Figure 10 compares the results of this study and the results of previous studies in References [28, 29, 33-46]. The modified catalyst P-21 required lower temperature and hydrogen pressure than the

other modified catalyst, which means that the cost of the experiment declined and the environmental impact was reduced. According to

the experimental results, the catalyst P-21 was the best catalyst for the preparation of aviation kerosene.

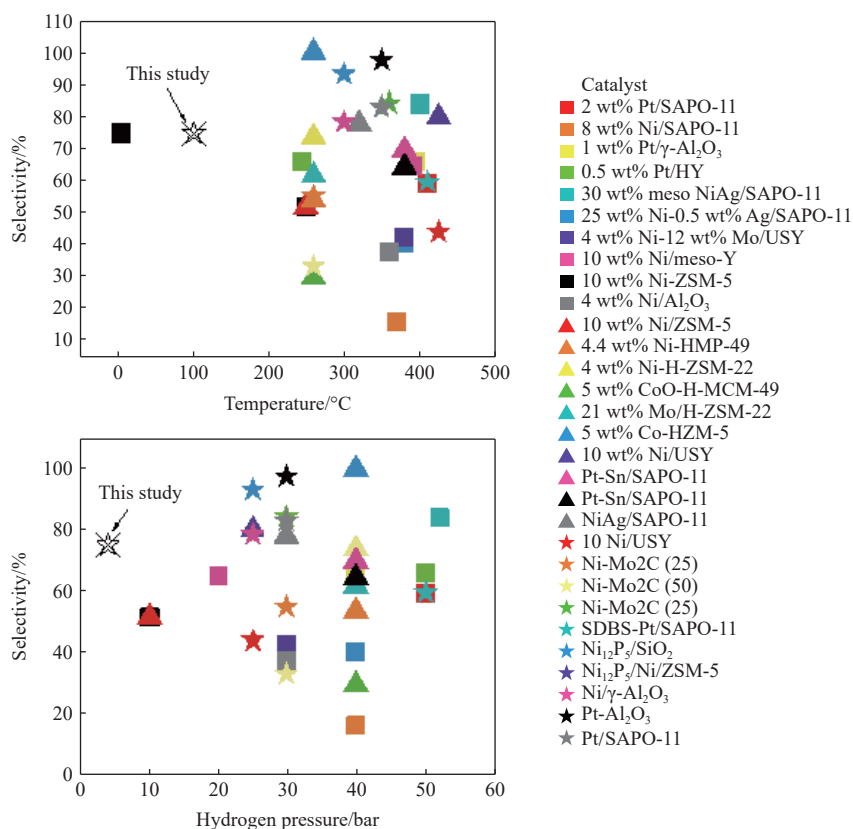


Figure 10 Experimental results of this study compared with previous studies

3.4 Reaction mechanism

According to the characterization and experimental results, the

photothermal catalytic reaction of Jatropha oil over the P-21 modified catalyst occurred as follows (Figure 11):

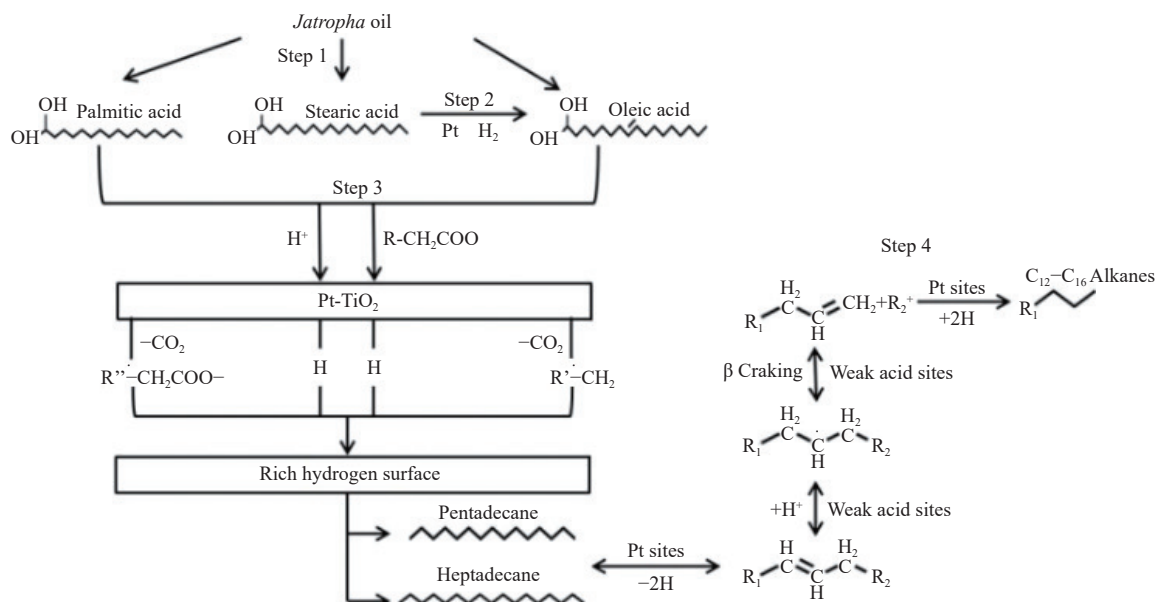


Figure 11 Mechanism of Jatropha oil to alkane fuel via photothermic catalysis

Step 1: Because of the adsorption of P-21, triglycerides were converted into fatty acids, such as oleic, stearic, and soft fatty acids under photothermal conditions;

Step 2: Unsaturated fatty acid molecules were adsorbed and migrated to Pt sites by molecular sieves under a low-hydrogen-pressure atmosphere, and formed as saturated fatty acids by direct

hydrogenation at the Pt sites;

Step 3: At the Pt-TiO₂ interface, saturated fatty acid molecules underwent photodecarboxylation under continuous light conditions and were reduced to hydrogen monomers and CO₂ gas, and left C_{n-1} alkyl radicals. At the same time, the proton reduction, hydrogen solubilization, and hydrogen spillover of Pt led to the formation of

hydrogen-rich surfaces on Pt and TiO₂, which accelerated the quenching of alkyl radicals by hydrogen to produce n-pentadecane and n-heptadecane^[10].

Step 4: Long-chain alkanes, such as heptadecane and pentadecane, were converted into C₁₂-C₁₆ alkanes by beta cleavage at weak acidic sites.

4 Conclusions

In this study, a scheme was proposed for the preparation of aviation kerosene from Jatropha oil according to photothermal coupling catalysis under mild conditions using six homemade catalysts: P-21, P-60, P-130, P-11, P-41, and PG with Jatropha oil as the raw material. The TiO₂ was compounded with molecular sieves by solid dispersion and solvent gelation methods and was doped with active metals by impregnation. The catalysts were characterized using XRD, HRTEM, N₂ adsorption and desorption, XRF, NH₃-TPD, and UV-Vis. By combining the characterization results with the previous experimental studies, we selected the optimal composite method, molecular sieve materials, and process parameters. Finally, the reaction mechanism involved in this study was inferred from the characterization and experimental results. The following conclusions can be drawn:

The preparation methods affect lattice types of TiO₂ on the catalysts, which further affects the catalyst performance. In the catalysts prepared by the solvent gel method, TiO₂ mostly existed in the form of amorphous TiO₂, and the products were easily agglomerated during the preparation process. This may have caused pore blockage inside the molecular sieve and may have reduced the catalytic performance. In contrast, the TiO₂ in the catalysts prepared by the solid dispersion method was 80% anatase TiO₂ and 20% rutile TiO₂, and thus was more suitable for the present reaction.

Between different molecular sieve materials, parameters such as pore size, specific surface area, and Si/Al ratio had a relatively important impact on the reaction results. It can be found that the HZSM-5 type molecular sieve with moderate specific surface area and smaller pore size had better performance. Because of a larger pore size, for the SAPO-11, MCM-41 molecular sieve, the reaction products may have entered the pore channel for cracking or other reactions, thus decreasing the selectivity of the target alkane. In addition, the HZSM-5 molecular sieve with a Si/Al ratio of 21 was more suitable for this reaction. The study showed that the material with a low Si/Al ratio had more weak acid sites, which had a catalytic effect on the cracking of the target alkane. In conclusion, P-21 was the most suitable catalyst for this study.

Acknowledgments

This work was financially supported by the National Natural Science Foundation of China (Grant No. 21868014), a Key Project of the Yunnan Fundamental Research Program (Study on Design of Novel Catalyst and Catalytic Process for Preparation of Bio-aviation Kerosene from Vegetable Oils Based on Photo-thermal Catalytic Technology), 2021 Low-carbon Development Guide Project of Yunnan Province, China (No. 135), Key S&T Project of China Tobacco Yunnan Industrial Co., Ltd., (Grant No. 2022GY03), Yunnan Academician and Expert Workstation (Grant No. 202205AF150024), Yunnan International S&T Cooperation Program, China (Grant No. 202003AF140001), Yunnan S&T Talents and Platform Program (Grant No. 202105AC160058) and Kunming International S&T Cooperation Base, China (Grant No. GHJD-2020026). Scientific research project of Yunnan Environmental Science Society, China (Grant No. XHKYKT006).

[References]

- [1] Alalwan H A, Alminshid A H, Aljaafari H A S. Promising evolution of biofuel generations. *Subject review. Renew Energy Focus*, 2019; 28: 127–139.
- [2] Blanco-Marigorta A M, Suárez-Medina J, Vera-Castellano A. Exergetic analysis of a biodiesel production process from *Jatropha curcas*. *Applied Energy*, 2013; 101: 218–225.
- [3] Xiao S, Fu Q, Li Z, Li J, Zhang L, Zhu X, et al. Solar-driven biological inorganic hybrid systems for the production of solar fuels and chemicals from carbon dioxide. *Renewable and Sustainable Energy Reviews*, 2021; 150: 111375.
- [4] Gabriel C B, Canhaci S J, Borges L E P, Fraga M A. Aviation biofuel range cycloalkane from renewables: Liquid-phase catalytic conversion of menthol on niobia-supported catalysts. *Fuel*, 2020; 277: 118288.
- [5] Macintosh A, Wallace L. International aviation emissions to 2025: Can emissions be stabilised without restricting demand? *Energy Policy*, 2009; 37(1): 264–273.
- [6] Bulushev D A, Ross J R H. Catalysis for conversion of biomass to fuels via pyrolysis and gasification: A review. *Catalysis Today*, 2011; 171(1): 1–13.
- [7] Yilmaz N, Atmanli A. Sustainable alternative fuels in aviation. *Energy*, 2017; 140(Part2): 1378–1386.
- [8] Qi Y, Wang J Y, Kou Y, Pang H C, Zhang S H, Li N, et al. Synthesis of an aromatic N-heterocycle derived from biomass and its use as a polymer feedstock. *Nature Communications*, 2019; 10: 2107.
- [9] Chen R X, Wang W C. The production of renewable aviation fuel from waste cooking oil. Part I: Bio-alkane conversion through hydro-processing of oil. *Renewable Energy*, 2019; 135: 819–835.
- [10] Huang Z P, Zhao Z T, Zhang C F, Lu J M, Liu H F, Luo N C, et al. Enhanced photocatalytic alkane production from fatty acid decarboxylation via inhibition of radical oligomerization. *Nature Catalysis*, 2020; 3: 170–178.
- [11] Eller Z, Varga Z, Hancsók J. Advanced production process of jet fuel components from technical grade coconut oil with special hydrocracking. *Fuel*, 2016; 182: 713–720.
- [12] Duan J Z, Han J X, Sun H, Chen P, Lou H, Zheng X M. Diesel-like hydrocarbons obtained by direct hydrodeoxygenation of sunflower oil over Pd/Al-SBA-15 catalysts. *Catalysis Communications*, 2012; 17: 76–80.
- [13] Kim S K, Brand S, Lee H S, Kim Y, Kim J. Production of renewable diesel by hydrotreatment of soybean oil: Effect of reaction parameters. *Chemical Engineering Journal*, 2013; 228: 114–123.
- [14] Horáček J, Tišler Z, Rubáš V, Kubička D. HDO catalysts for triglycerides conversion into pyrolysis and isomerization feedstock. *Fuel*, 2014; 121: 57–64.
- [15] Vásquez M C, Silva E E, Castillo E F. Hydrotreatment of vegetable oils: A review of the technologies and its developments for jet biofuel production. *Biomass and Bioenergy*, 2017; 105: 197–206.
- [16] Verma D, Rana B S, Kumar R, Sibi M G, Sinha A K. Diesel and aviation kerosene with desired aromatics from hydroprocessing of Jatropha oil over hydrogenation catalysts supported on hierarchical mesoporous SAPO-11. *Applied Catalysis A:General*, 2015; 490: 108–116.
- [17] Qin J, Li B S, Yan D. Synthesis, characterization and catalytic performance of well-ordered crystalline heteroatom mesoporous MCM-41. *Crystals*, 2017; 7(4): 89.
- [18] Xing G H, Liu S Y, Guan Q X, Li W. Investigation on hydroisomerization and hydrocracking of C₁₅-C₁₈ n-alkanes utilizing a hollow tubular Ni-Mo/SAPO-11 catalyst with high selectivity of jet fuel. *Catalysis Today*, 2019; 330: 109–116.
- [19] Kraeutler B, Bard A J. Heterogeneous photocatalytic decomposition of saturated carboxylic acids on titanium dioxide powder. Decarboxylative route to alkanes. *Journal of the American Chemical Society*, 1978; 9(52): 5985–5992.
- [20] Tijmensen M J A, Faaij A P C, Hamelinck C N, Van Hardeveld M R M. Exploration of the possibilities for production of fischer tropsch liquids and power via biomass gasification. *Biomass and Bioenergy*, 2002; 23(2): 129–152.
- [21] Kubacka A, Fernández-García M, Colón G. Advanced nanoarchitectures for solar photocatalytic applications. *Chemical Reviews*, 2012; 112: 1555–1614.
- [22] Vibhu S, Manpreet K, Sanjeev B. Performance investigation of high velocity flame sprayed multi-dimensional Ni-TiO₂ and Ni-TiO₂-Al₂O₃ coated hydro turbine steel under slurry erosion. *Wear*, 2020; 462–463: 203498.

- [23] Nie R F, Lei H, Pan S Y, Wang L N, Fei J H, Hou Z Y. Core-shell structured CuO-ZnO@HZSM-5 catalysts for CO hydrogenation to dimethyl ether. *Fuel*, 2012; 96: 419–425.
- [24] Wang Y D, Tao Z C, Wu B S, Xu J, Huo C F, Li K, et al. Effect of metal precursors on the performance of Pt/ZSM-22 catalysts for n-hexadecane hydroisomerization. *Journal of Catalysis*, 2015; 322: 1–13.
- [25] Mizukoshi Y, Makise Y, Shuto T, Hu J, Tominaga A, Shironita S, et al. Immobilization of noble metal nanoparticles on the surface of TiO₂ by the sonochemical method: Photocatalytic production of hydrogen from an aqueous solution of ethanol. *Ultrasonics Sonochemistry*, 2007; 14(3): 387–392.
- [26] Chiarello G L, Aguirre M H, Selli E. Hydrogen production by photocatalytic steam reforming of methanol on noble. *Journal of Catalysis*, 2010; 273(2): 182–190.
- [27] Chen Y B, Li X Y, Liu S J, Zhang W J, Wang Q, Zi W H. Effects of metal promoters on one-step Pt/SAPO-11 catalytic hydrotreatment of *castor* oil to C₈-C₁₆ alkanes. *Industrial Crops and Products*, 2020; 146: 112182.
- [28] Li X Y, Chen Y B, Hao Y J, Zhang X, Du J C, Zhang A M. Optimization of aviation kerosene from one-step hydrotreatment of catalytic *Jatropha* oil over SDBS-Pt/SAPO-11 by response surface methodology. *Renewable Energy*, 2019; 139: 551–559.
- [29] Gong S F, Shinozaki A, Shi M L, Qian E W. Hydrotreating of *Jatropha* oil over alumina based catalysts. *Energy and Fuels*, 2012; 26(4): 2394–2399.
- [30] Vichaphund S, Aht-ong D, Sricharoenchaikul V, Atong D. Effect of CV-ZSM-5, Ni-ZSM-5 and FA-ZSM-5 catalysts for selective aromatic formation from pyrolytic vapors of rubber wastes. *Journal of Analytical and Applied Pyrolysis*, 2017; 124: 733–741.
- [31] Kemdeo S M, Sapkal V S, Chaudhari G N. TiO₂-SiO₂ mixed oxide supported MoO₃ catalyst: Physicochemical characterization and activities in nitration of phenol. *Journal of Molecular Catalysis A:Chemical*, 2010; 323(1-2): 70–77.
- [32] Liu R H, Sarker M, Rahman M M, Li C, Chai M Y, Cotillon N R, et al. Multi-scale complexities of solid acid catalysts in the catalytic fast pyrolysis of biomass for bio-oil production-a review. *Progress in Energy and Combustion Science*, 2020; 80: 100852.
- [33] Shi Y C, Zhang J M, Xing E H, Xie Y B, Cao H B. Selective production of jet-fuel-range alkanes from palmitic acid over Ni/H-MCM-49 with two independent pore systems. *Industrial & Engineering Chemistry Research*, 2019; 58(47): 21341–21349.
- [34] Cao Y Y, Shi Y C, Bi Y F, Wu K J, Hu S J, Wu Y L, et al. Hydrodeoxygenation and hydroisomerization of palmitic acid over bi-functional Co/H-ZSM-22 catalysts. *Fuel Process Technology*, 2018; 172: 29–35.
- [35] Zhang J M, Shi Y C, Cao H B, Wu Y L, Yang M D. Conversion of palmitic acid to jet fuel components over Mo/H-ZSM-22 bi-functional catalysts with high carbon reservation. *Applied Catalysis A:General*, 2020; 608: 117847.
- [36] Du X Z, Zhou K Y, Zhou L Y, Lei X, Yang H R, Li D, et al. Efficient catalytic conversion of *Jatropha* oil to high grade biofuel on Ni-Mo₂C/MCM-41 catalysts with tuned surface properties. *Journal of Energy Chemistry*, 2021; 61: 425–435.
- [37] Hari T K, Yaakob Z. Production of diesel fuel by the hydrotreatment of *Jatropha* oil derived fatty acid methyl esters over γ -Al₂O₃ and SiO₂ supported NiCo bimetallic catalysts. *Reaction Kinetics Mechanisms and Catalysis*, 2015; 116(1): 131–145.
- [38] Zhang W J, Chen Y B, Zhuang S Y, Li R F, Hu L D. Acid-etched Pt/Al-MCM-41 catalysts for fuel production by one-step hydrotreatment of *Jatropha* oil. *GCB Bioenergy*, 2021; 13(4): 679–690.
- [39] da Rocha Filho G N, Brodzki D, Djéga-Mariadassou G. Formation of alkanes, alkylcycloalkanes and alkylbenzenes during the catalytic hydrocracking of vegetable oils. *Fuel*, 1993; 72(4): 543–549.
- [40] Jeong H, Bathula H B, Kim T W, Han G B, Jang J H, Jeong B, et al. Superior long-term stability of a mesoporous alumina-supported Pt catalyst in the hydrodeoxygenation of palm oil. *ACS Sustainable Chemistry & Engineering*, 2021; 9(3): 1193–1202.
- [41] Lin C H, Wang W C. Direct conversion of glyceride-based oil into renewable jet fuels. *Renewable and Sustainable Energy Reviews*, 2020; 132: 110109.
- [42] Chen L G, Li H W, Fu J Y, Miao C L, Lyu P M, Yuan Z H. Catalytic hydroprocessing of fatty acid methyl esters to renewable alkane fuels over Ni/HZSM-5 catalyst. *Catalysis Today*, 2016; 259(Part 2): 266–276.
- [43] Zhang Z W, Wang Q F, Chen H, Zhang X W. Hydroconversion of waste cooking oil into green biofuel over hierarchical USY-Supported NiMo catalyst: A comparative study of desilication and dealumination. *Catalysts*, 2017; 7(10): 281.
- [44] Cheng J, Zhang Z, Zhang X, Liu J F, Zhou J H, Cen K F. Hydrodeoxygenation and hydrocracking of microalgae biodiesel to produce jet biofuel over H₃PW₁₂O₄₀-Ni/hierarchical mesoporous zeolite Y catalyst. *Fuel*, 2019; 245: 384–391.
- [45] Feng F X, Niu X P, Wang L, Zhang X W, Wang Q F. TEOS-modified Ni/ZSM-5 nanosheet catalysts for hydroconversion of oleic acid to high-performance aviation fuel: Effect of acid spatial distribution. *Microporous and Mesoporous Materials*, 2020; 291: 109705.
- [46] Feng F X, Shang Z Y, Wang L, Zhang X W, Liang X H, Wang Q F. Structure-sensitive hydro-conversion of oleic acid to aviation-fuel-range-alkanes over alumina-supported nickel catalyst. *Catalysis Communications*, 2020; 134: 105842.